

An *a priori* analysis of a DNS database of turbulent lean premixed methane flames for LES with finite-rate chemistry

A. J. Aspden¹, N. Zettervall² and C. Fureby²

¹School of Engineering, Newcastle University, Stephenson Building,
Claremont Road, Newcastle-Upon-Tyne, NE1 7RU, UK

²Defence Security Systems Technology, The Swedish Defence Research Agency,
FOI, SE 147 25 Tumba, Stockholm, Sweden

2nd May 2018

Abstract

An *a priori* analysis of a DNS database of turbulent lean premixed methane flames is presented considering the relative effects of turbulence and LES filtering, along with a potential modelling approach for LES with finite-rate chemistry. The leading-order effect was found to be due to the filter operation; flame response to turbulence was a secondary effect, and manifested primarily as an increase in standard deviations about conditional means. It was found that the radicals O, H and OH were less impacted by the filter than other high-temperature radicals, which were significantly reduced in magnitude by the filter. By considering reaction path diagrams, key reactions have been identified that are responsible for disparities between the desired filtered reaction rates and the reaction rates evaluated using quantities available in LES calculations (i.e. the filtered species and temperature). More specifically, the hydrogen abstraction reactions that take CH₄ to CH₃ (by O, H and OH) were found to have particularly enhanced reaction rates, and dominate the reaction path. Under the conditions presented, reaction paths were found to be independent of turbulence intensity. In general, the filtered reaction rates from the DNS were found to align more closely with the filtered laminar profile than the reaction rate of filtered species and temperature, (but disparities were found to decrease with increasing Karlovitz number). A simple model for scaling reaction rates is considered based on filtered laminar flame profiles, and the resulting reaction paths demonstrate proof-of-concept of a simple approach for formulating a reaction rate model for LES with finite-rate chemistry.

1 Introduction

Predictive modelling of turbulent combustion incorporating finite-rate kinetics is becoming increasingly important for the development of fuel-flexible combustion devices with low emissions and high-speed propulsion systems. Large Eddy Simulation (LES) is a promising approach requiring closure models describing subfilter transport as for non-reactive flows [1], but also for filtered reaction rates, [2, 3, 4, 5]. Mixing and chemical reactions usually occur together on scales smaller than convection, requiring different modelling approaches, [4, 5]. These include flamelet models, e.g. [6], finite-rate chemistry models such as thickened flame models, [7], localized time-scale models, [8, 9, 10], approximate deconvolution models, [11], presumed Probability Density Function (PDF) models, [12], transported PDF models, [13, 14], Conditional Moment Closure (CMC) models, [15], and Linear Eddy Models (LEM), [16].

Assessment of flamelet and finite-rate chemistry models, e.g. [17, 18, 19, 20], have found satisfactory overall agreement for most models, but with finite-rate chemistry models performing somewhat better than the flamelet models. In finite-rate chemistry LES, the combustion chemistry is incorporated by solving filtered transport equations for the species, with the filtered reaction rates being computed either explicitly using filtered Arrhenius reaction rate expressions or tabulated reaction rates, [21]. An issue with finite-rate chemistry models is the dependence on the underlying reaction mechanism, [21, 22]. From [21, 22, 23] and other similar studies, it has been observed that skeletal reaction mechanisms can successfully be used in finite-rate chemistry LES.

The influence of the filtering is handled through different types of mathematical or phenomenological models, e.g. [7, 8, 9, 10, 11, 12, 13, 14, 15, 16], in conjunction with the reaction rates. The filtering operation has been examined previously for non-reacting LES (e.g. [24]), and for combustion LES [25] targetting tabulated chemistry based on presumed PDFs. Here, Direct Numerical Simulation (DNS) results from lean premixed methane-air flames will be used to examine the influence of the underlying turbulent flow on the filtered reaction rates, and hence the modelling requirements for finite-rate chemistry LES.

2 LES of Turbulent Combustion

LES equations of motion are derived from conservation of mass, momentum and energy by applying a low-pass filter. Physical processes on scales larger than the filter width, Δ , are resolved, whereas physics occurring on scales smaller than Δ require subfilter models. The full equation set can be found elsewhere (e.g. [4]), but the focus here is on the reaction terms appearing in the conservation of mass for species i ,

$$\frac{\partial}{\partial t} (\bar{\rho} \tilde{Y}_i) + \nabla \cdot (\bar{\rho} \tilde{Y}_i \tilde{\mathbf{v}}) = \nabla \cdot (D_i \nabla \tilde{Y}_i - \mathbf{b}_i) + \bar{\omega}_i, \quad (1)$$

in which, $\bar{\rho}$, $\tilde{\mathbf{v}}$, and \tilde{Y}_i are the (Favre) filtered density, velocity, and species mass fractions, respectively, D_i is the Fickian diffusion coefficient for species i , and the subfilter turbulent mixing is hidden in the diffusive flux term \mathbf{b}_i . The filtered reaction term $\bar{\omega}_i$ is the focus of the present work, in particular the non-linear response to the LES filtering operation, which can be written out to emphasize the dependencies on all dependent variables,

$$\bar{\omega}_i = M_i \sum_{j=1}^M (P''_{ij} - P'_{ij}) \bar{Q}_j, \quad (2)$$

where \bar{Q}_j are the filtered progress rates of reaction j ,

$$\bar{Q}_j = \overline{\left[k_{f,j} \prod_{k=1}^N \left(\frac{\rho Y_k}{M_k} \right)^{P'_{kj}} - k_{b,j} \prod_{k=1}^N \left(\frac{\rho Y_k}{M_k} \right)^{P''_{kj}} \right]}, \quad (3)$$

where $k_{f,j}$ and $k_{b,j}$ are the forward and backward rates of reaction j , respectively. Taylor series expansions of (3) have been discussed (from a RANS point of view) in [2], and this is not considered a useful approach for increasing the understanding of these terms or for the development of improved models due to the inherent non-linearities. Alternatively, by multiplying and dividing each of the reaction rates in (2) by the filtered reaction rates we have,

$$\bar{\omega}_i = M_i \sum_{j=1}^M (P''_{ij} - P'_{ij}) \Omega_j Q_j(\tilde{\mathbf{Y}}, \bar{T}), \quad (4)$$

in which $\Omega_j = \bar{Q}_j / Q_j(\tilde{\mathbf{Y}}, \bar{T})$ denote the correlations between the filtered reaction rates and the reaction rates evaluated by the filtered quantities accessible in LES. The correlations Ω_j then constitute a model approach for LES with finite-rate chemistry. The premise of the present work is to evaluate factors affecting these correlation terms for a range of lean premixed flames at different Ka to investigate the influence of the turbulence on the combustion chemistry, and thus also obtain information about the subfilter modelling requirements for finite-rate chemistry LES.

3 DNS of Turbulent Premixed Methane Flames

The simulation database that will be used for the present study consists of a series of DNS with detailed chemistry of statistically-stationary statistically-planar turbulent premixed methane flames

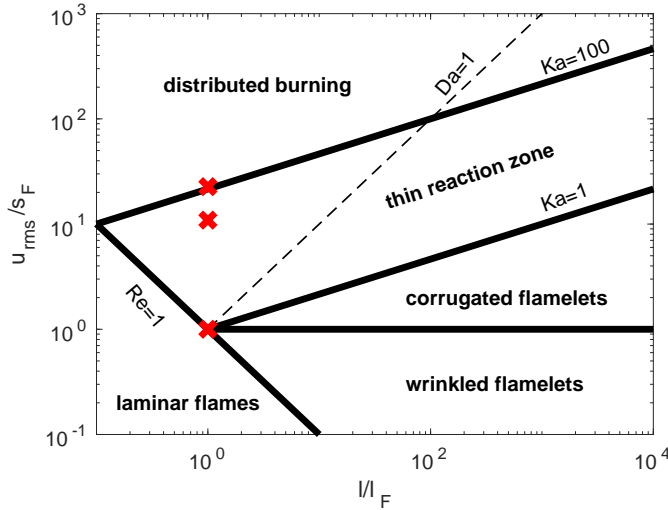


Figure 1: Regime diagram showing the conditions analysed.

in maintained homogeneous isotropic turbulence, [26, 27, 28]. The simulations were run using the well-established low Mach number combustion solver developed at the Center for Computational Sciences and Engineering at the Lawrence Berkeley National Laboratory. The details of the numerical method can be found in [29] and [30]. The methodology treats the fluid as a mixture of perfect gases, using a mixture-averaged model for diffusive transport, ignoring Dufour and Soret effects. A long-wavelength forcing term designed to establish and maintain turbulence with the desired properties [31]. The chemical kinetics and transport were modelled using the GRIMech 3.0 without emissions chemistry [32], resulting in 35 species with 217 elementary reactions. The simulations were conducted at $\Lambda = l/l_F = 1$, as part of the study reported in [27], matching the Karlovitz numbers of the $\Lambda = 4$ calculations reported in [26] ($Ka = (u^3 l_F)/(s_F^3 l) = 1$ and 36), along with a higher Karlovitz number case from [28] ($Ka = 108$) looking at more turbulent conditions. The conditions are shown on the regime diagram in figure 1, and span the conventionally-defined thin reaction zone. As with all DNS studies, the integral length scale has been sacrificed to resolve the flame adequately, but is sufficient for studying small-scale turbulence-chemistry interaction, and is representative of high intensity turbulence that would reach these scales through the energy cascade from larger integral lengths at the same Karlovitz numbers.

4 Analysis of the DNS Data

The DNS data were filtered using a simple top-hat box filter with a width approximately equal to one flame thermal thickness; at approximately 660 microns, this filter width is typical for combustion LES (e.g. [19]), and much larger than the scales over which the reactions take place. A quantity q filtered in this way will be denoted as \bar{q} , with Favre filtered quantities denoted $\tilde{q} = \overline{\rho q}/\bar{\rho}$. Comparisons are made between the reaction rates Q_j , the filtered reaction rates \bar{Q}_j and the reaction rates evaluated using filtered species and temperature $Q_j(\tilde{Y}, \tilde{T})$. Each of these three kinds of reaction rates was evaluated for a laminar flame profile (i.e. a steady unstrained one-dimensional flame) and for the DNS data, from which a temporally-averaged mean and standard deviation was evaluated conditioning on temperature.

The effect of turbulence and the filtering procedure on some representative species is presented in figure 2 as two-dimensional slices; all species at all Ka are presented in the supplementary material. As expected, the turbulence has little effect at $Ka = 1$ other than producing large-scale wrinkling. At $Ka = 108$, turbulence has a significant effect on the flame, especially on the preheat region, which is substantially thickened (e.g. CH_4). Turbulence also increases the occurrence of highly-curved regions, which leads to variation along the flame surface and a slightly enhanced radical pool (e.g. H). Further details of flame response to turbulence in these cases can be found in [26, 27, 28]. Naturally, the filter smooths out monotonic fields like fuel mass fraction, but has a more significant effect particularly on

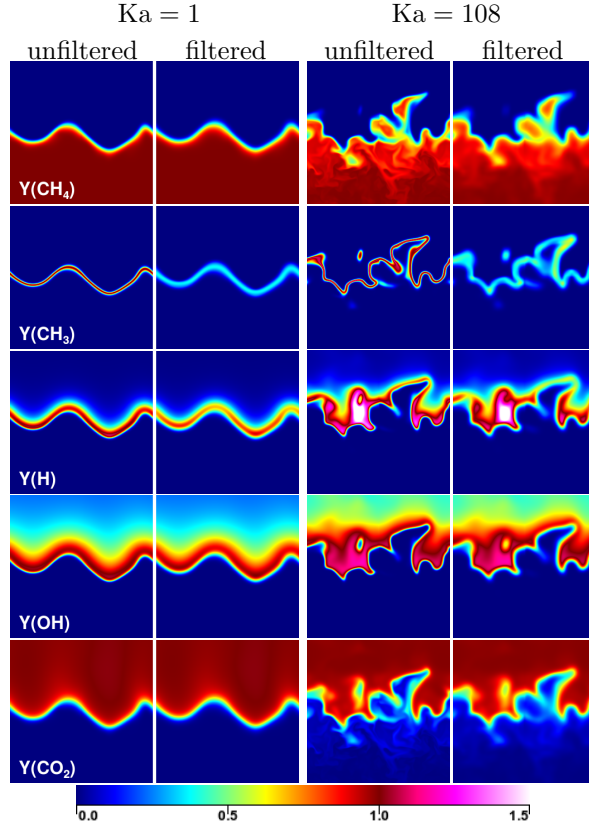


Figure 2: Two-dimensional slices comparing the effect of the filter at $Ka = 1$ and 36; all fields are normalised by corresponding laminar values, and periodicity has been exploited to join x and y slices together to show more flame surface. Each square panel is 20 flame thickness in size.

the thickness and magnitude of narrow fields such as CH_3 . At high Ka , the radicals H and OH appear less impacted by the filter, and present values in excess of the laminar values (as seen by the magenta and white regions).

The response of species distribution to turbulent mixing was classified in [26], and the response to the filtering operation has been found to be consistent with this classification; all species profiles for all Ka are presented by classification in the supplementary material, but the profiles for CH_4 , CH_3 , H and OH at $Ka = 108$ are presented in figure 3. At low Ka (again see supplementary material), the conditional means align closely with the laminar profiles, and the standard deviations are small. The main response to increasing the Karlovitz number, is an increase in the standard deviations for intermediate species (see dashed lines in figure 3). The filtered profiles are more interesting, and depend on temperature, Karlovitz number, and species type. Reactants and products (see supplementary data) present filtered profiles that, at low-to-moderate temperatures, align with the unfiltered turbulent profile (it is likely that both actually align with the unity Lewis number profile); at higher temperatures, however, there is a deviation from the other profiles (specifically, an increase in fuel mass fraction and a decrease in water mass fraction), the explanation for which is currently unclear. The alignment at low temperatures is attributed to penetration of turbulence into the preheat region, broadening the profiles in physical space. The conditional means of the radicals O , H and OH increase, whereas almost all of the other carbonated radicals (represented here by CH_3) remain close to the laminar profile. A significant difference is observed in response to the filter operation; a substantial decrease in the peak value is observed in the short-lived high-temperature radicals, but is much less pronounced for O , H and OH , which present increased profiles at lower temperatures.

Before considering individual reactions, the effect of the filter on the overall reaction paths are considered. Path diagrams for $Ka = 108$ are shown in figure 4 for carbon (top), and oxygen (bottom), with the unfiltered DNS data on the left, and reaction rates based on filtered species/temperature DNS data on the right (note that the reaction path diagram of filtered reactions is not presented as

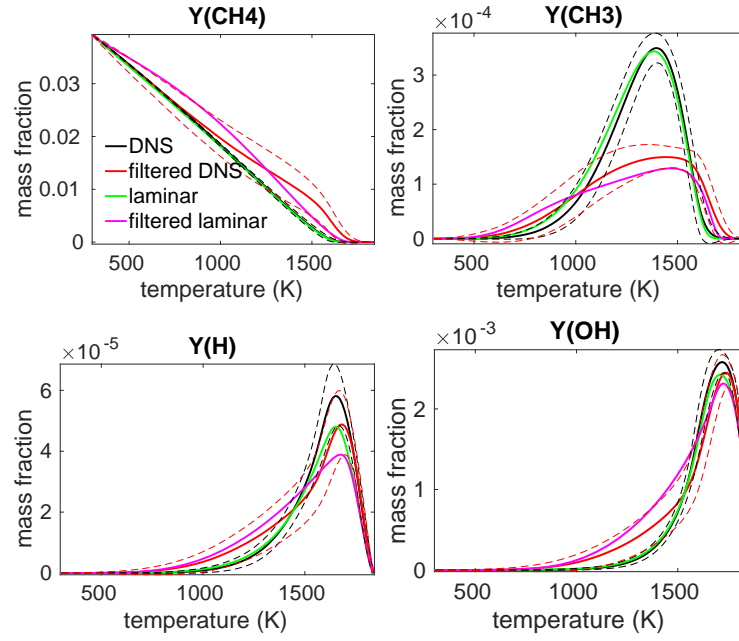


Figure 3: Conditional means of unfiltered and filtered species mass fractions for $Ka = 108$. One standard deviation about the mean are shown by dashed lines of corresponding colour. Note that the filtered profiles are conditioned on filtered temperature.

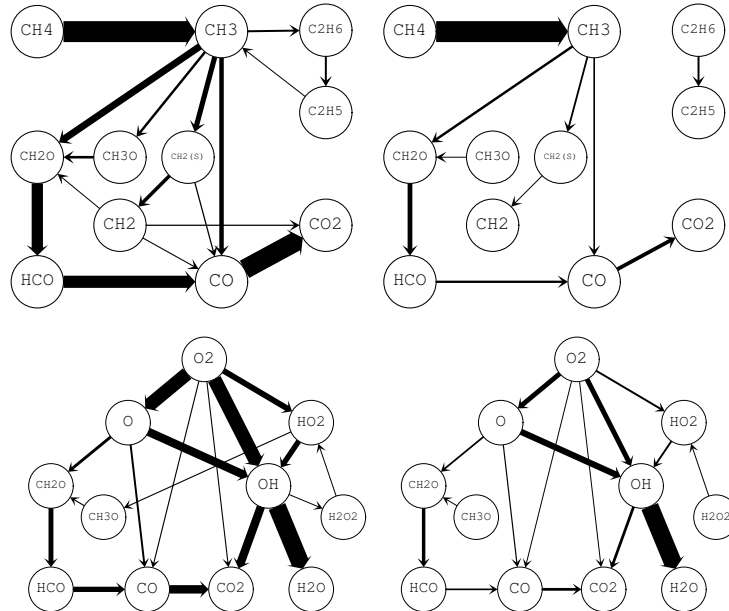


Figure 4: Reaction path diagrams following carbon (top) and oxygen (bottom); unfiltered DNS data on the left, and reaction rates based on filtered species/temperature DNS data on the right.

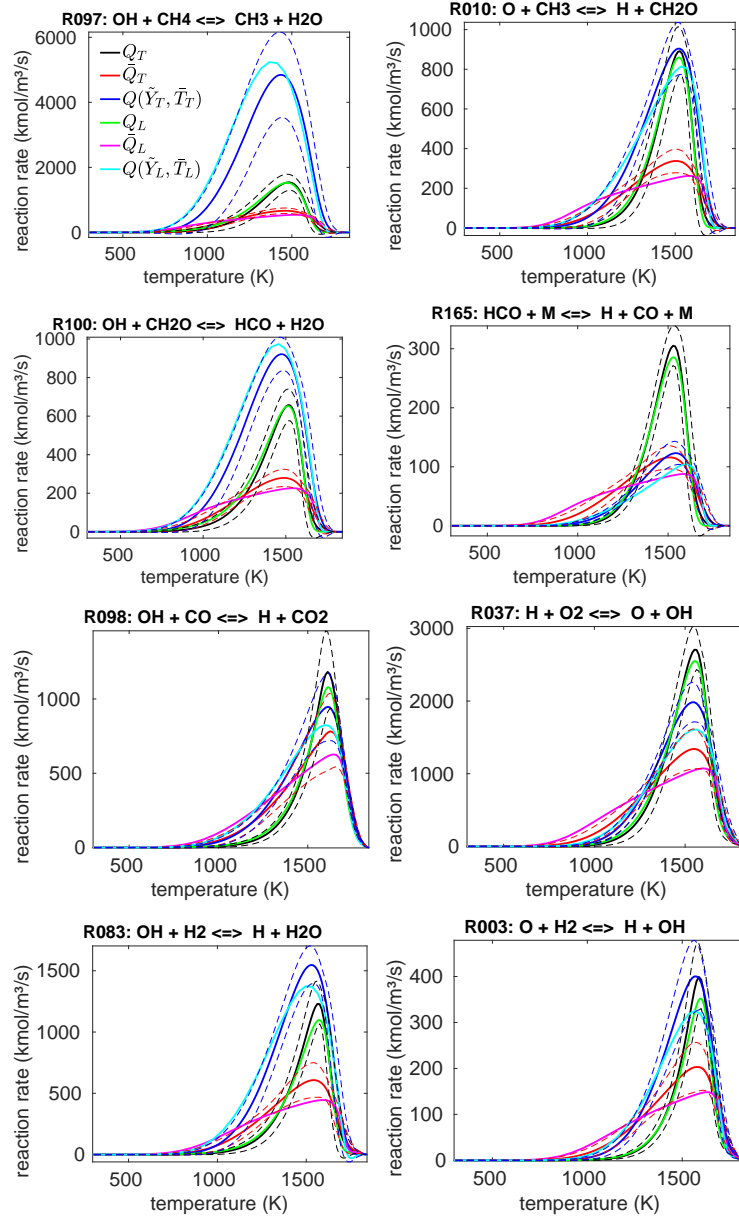


Figure 5: Conditional means of filtered and unfiltered reaction rates for $Ka = 108$ and laminar flames. Note that the filtered profiles are conditioned on filtered temperature.

the operation used to construct the reaction paths integrates out the effect of the filter). The size of each arrow reflects the rate of atom transfer normalised by the peak rate, and only rates greater than 2% of the peak are shown. (Note that missing links do not indicate that the reactions are not present, they have just fallen below the cut-off threshold based on the peak reaction rate.) It is clear that the filter changes the balance of reaction paths significantly; following carbon, the main decomposition of CH_4 to CH_3 far exceeds all of the other rates, and following oxygen the final step of OH to H_2O becomes dominant. The same response was observed for all Karlovitz numbers (see supplementary material, which also includes path diagrams following hydrogen); the effect of the filter on the reaction rates appears to be largely independent from Karlovitz number for these conditions.

Profiles of the key reaction rates are presented in figure 5 based on the main pathway from the reaction path diagrams ($CH_4 \rightarrow CH_3 \rightarrow CH_2O \rightarrow HCO \rightarrow CO \rightarrow CO_2$); again, all reactions for all Karlovitz numbers are included as supplementary material for completeness. In each plot, six reaction rate profiles are presented for unfiltered rates Q_L and Q_T , filtered rates \bar{Q}_L and \bar{Q}_T , and rates evaluated with filtered species/temperature $Q(\bar{Y}_L, \bar{T}_L)$ and $Q(\bar{Y}_T, \bar{T}_T)$, where suffices L and T denote laminar and turbulent profiles, respectively; standard deviations are shown by dashed lines for turbulent cases.

The main reactions responsible for fuel consumption are hydrogen abstraction by O , H , and OH ,

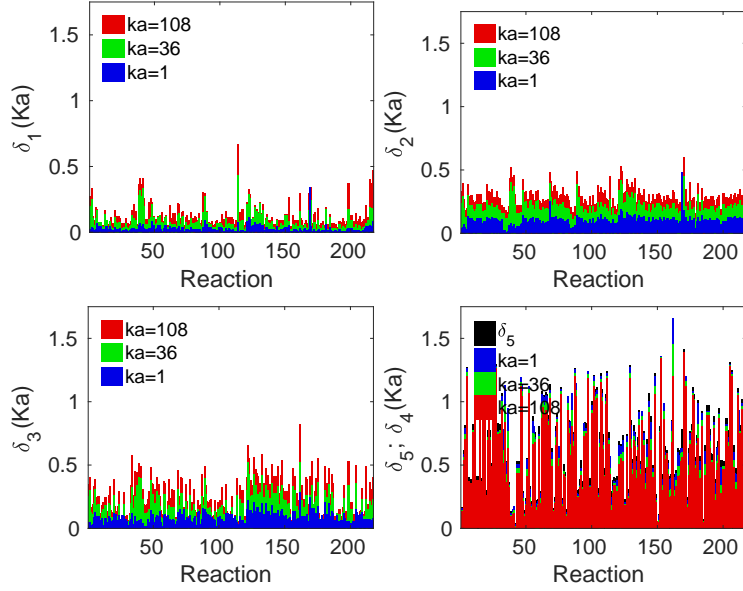


Figure 6: Difference metrics δ_i for all turbulent cases.

the latter is shown by R097 in figure 5, but is representative of the other two reactions (see R011 and R052 in the supplementary material). The conditional mean of the turbulent profile (black) aligns closely with the laminar profile (green), with similar alignment between the filtered profiles (red and magenta). The reaction rates of the filtered species/temperature (blue and cyan) are significantly different from the other two pairs of profiles; the effects of non-linearities in reaction rates profoundly affects all three abstraction reactions, and explains the dominance of the $\text{CH}_4 \rightarrow \text{CH}_3$ step in the carbon (and hydrogen) path diagrams of the filtered data.

The main reaction in the next step in the carbon path ($\text{CH}_3 \rightarrow \text{CH}_2\text{O}$) is R010. Once again, the reactions align closely in pairs, and while the reaction rates of filtered species/temperature are high, they are not as significantly different as in the abstraction reactions. The $\text{CH}_2\text{O} \rightarrow \text{HCO}$ step is represented here by R100 (see also R015 and R057 in the supplementary material), and shows an increase in reaction rates of filtered species/temperature with a magnitude between that observed in R100 and the abstraction reactions. The $\text{HCO} \rightarrow \text{CO}$ step (R165 presented here; see also R164 and R166 in the supplementary material) does not see a significant increase in magnitude of reaction rate, nor does the main oxidation step $\text{CO} \rightarrow \text{CO}_2$ (R098).

The key reactions in the oxygen path diagram are R037, which takes O_2 to both O and OH, R083, which takes OH to H_2O (and H_2 to H), and R003 which take O to OH (and again H_2 to H); the latter stages of carbon oxidation are discussed above (R100, R165 and R098). In R037, the effects of non-linearities are less pronounced than R083 (or the early stages in the carbon path), which explains the shift observed in the oxygen path diagram towards R083. Again the reaction rate of filtered species/temperature (blue) aligns more closely with the corresponding laminar profile (cyan) than the turbulent filtered reaction profile (red).

For the reactions in general, it appears that in many cases, but by no means all, the profiles loosely align in pairs; specifically, the conditional mean of the turbulent data (black) aligns with the laminar profile (green), the filtered turbulent data (red) aligns with the filtered laminar profile (magenta), and the reaction rate of filtered turbulent species/temperature (blue) aligns with the reaction rates of the filtered laminar profile (cyan). There are other reaction rates with interesting response to filtering (for example, see R033, R114 and R124 in the supplementary material), especially those involving HO_2 , H_2O_2 or CH_3O , but these are less significant reactions in the overall mechanism.

To quantify the alignment of the different reaction profiles, first define a normalised difference between two functions $f(T)$ and $g(T)$ as

$$\delta(f, g) = \sqrt{\int (f - g)^2 dT \bigg/ \frac{1}{2} \int f^2 + g^2 dT},$$

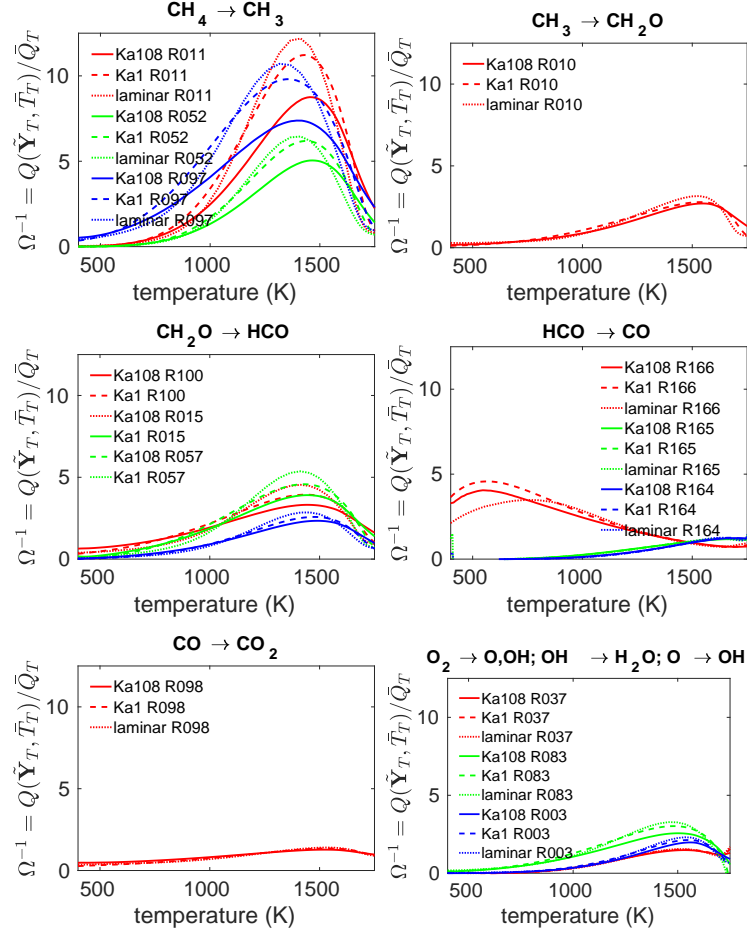


Figure 7: Conditional means of reciprocals of reaction rate ratios, $\Omega_j^{-1} = Q_j(\tilde{Y}, \tilde{T})/\bar{Q}_j$.

and then define five differences

$$\begin{aligned}\delta_1 &= \delta(Q_T, Q_L), & \delta_2 &= \delta(\bar{Q}_T, \bar{Q}_L), \\ \delta_3 &= \delta(Q(\tilde{Y}_T, \tilde{T}_T), Q(\tilde{Y}_L, \tilde{T}_L)), \\ \delta_4 &= \delta(Q(\tilde{Y}_T, \tilde{T}_T), \bar{Q}_T), & \delta_5 &= \delta(Q(\tilde{Y}_L, \tilde{T}_L), \bar{Q}_L).\end{aligned}$$

These five differences are depicted by bar graphs in figure 6 for each Karlovitz number. This comparison clearly demonstrates that the laminar-turbulent pairs of profiles from figures 3 and 5 (black and green by δ_1 , red and magenta by δ_2 , and blue and cyan by δ_3) are more closely aligned than the filtered reactions (red, magenta) and the reaction of filtered species/temperature (blue, cyan) in both turbulent and laminar differences (δ_4 , δ_5). Interestingly, the laminar difference δ_5 is generally larger than all of the turbulent differences δ_4 , which actually decreases with increasing Ka.

From a modelling point of view, the ratio of the filtered reaction rate to the reaction rate of filtered species/temperature was defined as $\Omega_j = \bar{Q}_j/Q_j(\tilde{Y}, \tilde{T})$. Figure 7 plots the reciprocal of Ω_j for the key reactions plotted in figure 5, along with other corresponding reactions in the key steps; the reciprocal is used as it was found to tend to zero on both sides of the flame. Once again, the strongest response is observed in the hydrogen abstraction reactions R011, R052 and R097. Perhaps surprisingly, there appears to be relative insensitivity to turbulence intensity; furthermore, the profiles from the filtered laminar flame have also been plotted as dotted lines, and are reasonably close to the turbulent profiles. This suggests that a potential turbulence modelling approach is to derived values for Ω_j based on the laminar flame.

Notwithstanding the temperature dependence of Ω_j , a model constant $\hat{\Omega}_j$ can be defined for each

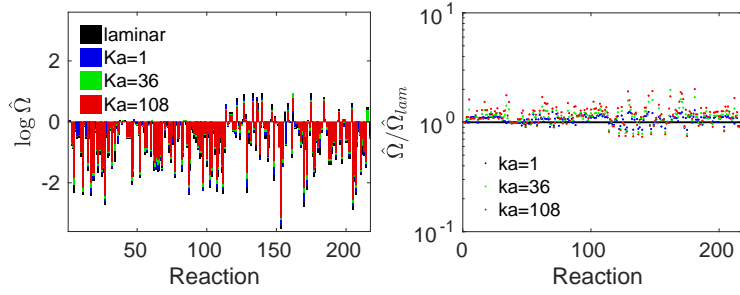


Figure 8: Left: model values of $\log \hat{\Omega}_j$. Right: $\hat{\Omega}_{j,T} / \hat{\Omega}_{j,L}$.

reaction as

$$\hat{\Omega}_j = \frac{\max_T |\bar{Q}_j|}{\max_T |Q_j(\tilde{Y}, \tilde{T})|}. \quad (5)$$

This represents a simple scaling of each reaction based on the ratio of filtered reaction rate to reaction rate of filtered species and temperature; note that the errors introduced through this approximation will be greatest away from the flame where the reactions go to zero, and so are expected to be of little importance. The log of $\hat{\Omega}_j$ is presented in figure 8, which gives equal weighting to reactions that need to be enhanced (positive values) and those the need to be suppressed (negative values). The values are predominantly negative, indicative that $Q_j(\tilde{Y}, \tilde{T})$ is generally higher than \bar{Q}_j . Pronounced negative values are found for the abstraction reactions considered above, along with those for ethane and propane (e.g. R0027, R205 and R207), and some other reactions involving CH_3O (e.g. R017 and R153). Pronounced positive values appear to involve species and reactions that have narrow profiles, and so are smeared by the filter (e.g. R122, R127, R133, R140, and R175). Again, note that there is relative insensitivity to Ka , and typically, the highest Ka corresponds to the smaller values of $\log \hat{\Omega}_j$. Scaling the turbulent $\hat{\Omega}_{j,T}$ by the corresponding laminar value, $\hat{\Omega}_{j,L}$, as shown in the right-hand panel of figure 8, further demonstrates a surprising insensitivity to turbulence conditions.

This suggests that it may be possible to formulate a model for $\hat{\Omega}_j$ based on filtered laminar profiles alone. To examine this potential, reaction path diagrams are presented in figure 9 that use filtered species and temperature from the $Ka = 108$ case with reaction rates modified using $\hat{\Omega}_{j,L}$ from the laminar flame profiles. Compared with the corresponding plots on the figure 4 the modified reaction paths align much more closely with the filtered reaction rates than the reaction rates of the filtered species and temperature. There are some clear differences; the $\text{CH}_4 \rightarrow \text{CH}_3$ edge is thinner in figure 9, and there are some new reaction paths present in the oxygen path in figure 9 (e.g. $\text{O}_2 \rightarrow \text{CH}_2\text{O}$ and $\text{HO}_2 \rightarrow \text{CH}_3\text{O}$). These differences suggest that the balance has not been completely restored by the model $\hat{\Omega}_{j,L}$, and the normalisation hides the overall reaction rates (which can be easily tuned), but this example provides proof-of-concept that a simple scaling of reaction rates by $\hat{\Omega}_{j,L}$ based on filtered laminar profiles is a straightforward approach that may yield feasible flame models for LES with finite-rate chemistry.

5 Discussion and Conclusions

An *a priori* analysis of a DNS database of turbulent lean premixed methane flames has been presented. The leading-order effect was found to be due to the filter operation, and flame response to turbulence was a secondary effect (figure 6), which manifested primarily as an increase in standard deviation; moreover, with increasing Karlovitz number, the disparity (as represented by δ_4) was found to decrease. Species profiles (figure 3) were found to align with the classification presented in [26]. Importantly, the radicals O, H and OH were found to be less impacted by the filter than other high-temperature radicals, which were significantly reduced in magnitude by the filter. It is the non-linear response in the reaction progress rates that presents the main modelling challenge (figure 5). By considering reaction path diagrams, key reactions have been identified that are responsible for disparities between the desired filtered reaction rates and the reaction rates evaluated using quantities available in LES

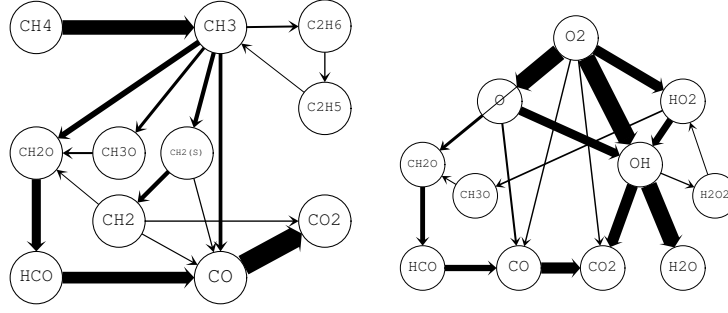


Figure 9: Reaction path diagrams following carbon (left) and oxygen (right) using the model values of $\hat{\Omega}_{j,L}$ and filtered species and temperature from the $Ka = 108$ case.

calculations (i.e. the filtered species and temperature). Specifically, the hydrogen abstraction reactions that take CH_4 to CH_3 (by O, H and OH) were found to have a particularly enhanced reaction rate, and dominate the whole reaction path diagram. Under the conditions presented, reaction paths were found to be largely independent of turbulence intensity. In general, reaction rates were found to align in pairs; i.e. the turbulent profile Q_T aligned with the laminar profile Q_L , the filtered profiles \bar{Q}_T aligned with \bar{Q}_L , and the reaction rate of filtered quantities $Q(\tilde{Y}_T, \tilde{T}_T)$ aligned with $Q(\tilde{Y}_L, \tilde{T}_L)$, (see figure 6). This alignment and relative insensitivity to Ka suggests that a model for the reaction rate scalings (e.g. $\hat{\Omega}_{j,L}$) can be formulated based on filtered laminar profiles. To this end, an example was considered by taking the ratio of the maximum absolute values, from which reaction paths were formed that presented better agreement with the actual reaction paths than those evaluated using filtered species and temperature. The example given is not intended to be a model proposal, and much more work is required to develop this concept into a predictive model. In particular, further work is required to consider a broader range of conditions (e.g. other fuels, Lewis number effects, and turbulent conditions), and the effect of the filter width (and form). Moreover, such *a priori* analysis is a long way from a predictive model that will perform well in practice; it is anticipated that the simple approach proposed here will perform poorly without further calibration. Fine tuning the model constants for reaction rates could be performed by some kind of automated approach. Finally, confirmation of the approach will have to come from successful *a posteriori* testing, but the present paper demonstrates proof-of-concept of a potential approach for formulating a reaction rate model for LES with finite-rate chemistry, and highlights the possibility of being able to base the approach on filtered laminar flames.

Acknowledgments

CF and NZ acknowledge the financial support from the Swedish Armed forces and by the Swedish Energy Agency via the EFFECT2 project. The authors are also grateful to John Bell and Marc Day for computational support.

References

- [1] Pierre Sagaut. *Large eddy simulation for incompressible flows: an introduction*. Springer Science & Business Media, 2006.
- [2] Thierry Poinot and Denis Veynante. *Theoretical and numerical combustion*. RT Edwards, Inc., 2005.
- [3] J Janicka and A Sadiki. Large eddy simulation of turbulent combustion systems. *Proceedings of the Combustion Institute*, 30(1):537–547, 2005.
- [4] Tarek Echekki. Multiscale methods in turbulent combustion: strategies and computational challenges. *Computational Science & Discovery*, 2(1):013001, 2009.

- [5] Suresh Menon and Christer Fureby. Computational combustion. *Encyclopedia of Aerospace Engineering*, 2010.
- [6] ER Hawkes and RS Cant. A flame surface density approach to large-eddy simulation of premixed turbulent combustion. *Proceedings of the Combustion Institute*, 28(1):51–58, 2000.
- [7] O Colin, F Ducros, D Veynante, and Thierry Poinso. A thickened flame model for large eddy simulations of turbulent premixed combustion. *Physics of Fluids*, 12(7):1843–1863, 2000.
- [8] C Fureby. Large eddy simulation modelling of combustion for propulsion applications. *Philosophical Transactions of the Royal Society of London A: Mathematical, Physical and Engineering Sciences*, 367(1899):2957–2969, 2009.
- [9] Eugenio Giacomazzi, Claudio Bruno, and Bernardo Favini. Fractal modelling of turbulent combustion. *Combustion Theory and Modelling*, 4(4):391–412, 2000.
- [10] Vladimir Sabelnikov and Christer Fureby. LES combustion modeling for high Re flames using a multi-phase analogy. *Combustion and Flame*, 160(1):83–96, 2013.
- [11] Joseph Mathew. Large eddy simulation of a premixed flame with approximate deconvolution modeling. *Proceedings of the Combustion Institute*, 29(2):1995–2000, 2002.
- [12] P Gerlinger. Investigation of an assumed PDF approach for finite-rate chemistry. *Combustion Science and Technology*, 175(5):841–872, 2003.
- [13] G Bulat, WP Jones, and AJ Marquis. Large eddy simulation of an industrial gas-turbine combustion chamber using the sub-grid PDF method. *Proceedings of the Combustion Institute*, 34(2):3155–3164, 2013.
- [14] Jeonglae Kim and Stephen B Pope. Effects of combined dimension reduction and tabulation on the simulations of a turbulent premixed flame using a large-eddy simulation/probability density function method. *Combustion Theory and Modelling*, 18(3):388–413, 2014.
- [15] S Navarro-Martinez, A Kronenburg, and F Di Mare. Conditional moment closure for large eddy simulations. *Flow, Turbulence and Combustion*, 75(1-4):245–274, 2005.
- [16] Suresh Menon and Alan R Kerstein. The linear-eddy model. *Turbulent Combustion Modeling*, pages 221–247, 2011.
- [17] FE Hernández-Pérez, FTC Yuen, CPT Groth, and ÖL Gülder. LES of a laboratory-scale turbulent premixed bunsen flame using FSD, PCM-FPI and thickened flame models. *Proceedings of the Combustion Institute*, 33(1):1365–1371, 2011.
- [18] T Ma, OT Stein, N Chakraborty, and AM Kempf. A posteriori testing of the flame surface density transport equation for LES. *Combustion Theory and Modelling*, 18(1):32–64, 2014.
- [19] Christer Fureby. A comparative study of large eddy simulation (LES) combustion models applied to the Volvo validation rig. In *55th AIAA Aerospace Sciences Meeting, AIAA SciTech Forum, AIAA*, volume 1575, 2017.
- [20] E Fedina, C Fureby, G Bulat, and W Meier. Assessment of finite rate chemistry large eddy simulation combustion models. *Flow, Turbulence and Combustion*, pages 1–25, 2017.
- [21] G Bulat, E Fedina, C Fureby, W Meier, and U Stopper. Reacting flow in an industrial gas turbine combustor: LES and experimental analysis. *Proceedings of the Combustion Institute*, 35(3):3175–3183, 2015.
- [22] N Zettervall, K Nordin-Bates, EJK Nilsson, and C Fureby. Large eddy simulation of a premixed bluff body stabilized flame using global and skeletal reaction mechanisms. *Combustion and Flame*, 179:1–22, 2017.

- [23] Benoit Fiorina, O Gicquel, L Vervisch, S Carpentier, and N Darabiha. Premixed turbulent combustion modeling using tabulated detailed chemistry and PDF. *Proceedings of the Combustion Institute*, 30(1):867–874, 2005.
- [24] Shewen Liu, Charles Meneveau, and Joseph Katz. On the properties of similarity subgrid-scale models as deduced from measurements in a turbulent jet. *Journal of Fluid Mechanics*, 275:83–119, 1994.
- [25] S. Lapointe and G. Blanquart. A priori filtered chemical source term modeling for les of high karlovitz number premixed flames. *Combust. Flame*, 176:500–510, 2017.
- [26] A. J. Aspden, M. S. Day, and J. B. Bell. Three-dimensional direct numerical simulation of turbulent lean premixed methane combustion with detailed kinetics. *Combustion and Flame*, 166:266–283, 2016.
- [27] A. J. Aspden, J. B. Bell, M. S. Day, and F. N. Egolfopoulos. Turbulence–flame interactions in lean premixed dodecane flames. *Proceedings of the Combustion Institute*, 36(2):2005–2016, 2017.
- [28] A. J. Aspden, M. S. Day, and J. B. Bell. Towards distributed burning in turbulent premixed flames. *Submitted*, 2018.
- [29] M. S. Day and J. B. Bell. Numerical simulation of laminar reacting flows with complex chemistry. *Combust. Theory Modelling*, 4:535–556, 2000.
- [30] A. Nonaka, J. B. Bell, M. S. Day, C. Gilet, A. S Almgren, and M. L. Minion. A deferred correction strategy for low mach number flow with complex chemistry. *Combust. Theory Modelling*, 16(6):1053–1088, 2012.
- [31] A. J. Aspden, N. Nikiforakis, S. B. Dalziel, and J. B. Bell. Analysis of Implicit LES methods. *Comm. App. Math. Comput. Sci.*, 3(1):101, December 2008b.
- [32] M. Frenklach, H. Wang, M. Goldenberg, G. P. Smith, D. M. Golden, C. T. Bowman, R. K. Hanson, W. C. Gardiner, and V. Lissianski. GRI-Mech—an optimized detailed chemical reaction mechanism for methane combustion. Technical Report GRI-95/0058, Gas Research Institute, 1995. http://www.me.berkeley.edu/gri_mech/.